Supporting Information

Manuscript: **Towards Robust Alkane Oxidation Catalysts: Electronic Variations in Non-Heme Iron(II) Complexes and their Effect in Catalytic Alkane Oxidation**

Authors: Jason England, Reema Gondhia, Laura Bigorra-Lopez, Allan R. Petersen, George J.P. Britovsek and Andrew J.P. White

Experimental Details

VT Magnetic Susceptibility measurements via the Evans' NMR method

Magnetic susceptibilites in CD_2Cl_2 and CD_3CN solution at 298 K were determined by the Evans' Method.[1-4] Variable temperature magnetic moment determinations in acetonitrile solution were carried according to the methods described previously,[5, 6] using either a Bruker 400 MHz or Bruker 500 MHz spectrometer and a 5mm Wilmad Coaxial Insert NMR tube. Corrections for the change in solvent density with temperature were applied according to the data provided for CH_3CN[7] and an additional factor (0.844/0.786) for the difference between the densities of CD_3CN (δ = 0.844 g/ml at 298K) and CH_3CN (δ = 0.786 g/ml at 298K) was applied. The concentration of the samples was kept under 15 mM. Diamagnetic corrections were found insignificant and were not applied.

1. Evans, D. F., *J. Chem. Soc.* **1959**, *36*, 2003.
2. Evans, D. F.; Fazakerley, G. V.; Phillips, R. F., *J. Chem. Soc.* **1971**, *A*, 1931.
3. Evans, D. F.; Jakubovic, D. A., *J. Chem. Soc., Dalton Trans.* **1988**, 2927.
4. Grant, D. H., *J. Chem. Educ.* **1995**, *72*, 39.
5. Bryliakov, K. P.; Duban, E. A.; Talsi, E. P., *Eur. J. Inorg. Chem.* **2005**, 72.
6. Turner, J. W.; Schultz, F. A., *Inorg. Chem.* **2001**, *40*, 5296.
7. Kratze, H.; Müller, S., *J. Chem. Thermodyn.* **1985**, *17*, 151.

Standard Testing Conditions for the Oxidation of Cyclohexane.

Catalytic oxidations were all run at room temperature. The reaction products were analysed by GC analysis, using GC-MS for product identification. All catalytic data quoted is the average of at least two runs. 2.1 mmol (0.23 mL) of cyclohexane was added to a 75x25 mm sample vial containing 2.1 μmol of complex dissolved in 2.7 mL of acetonitrile and a

small egg-shaped stirrer bar, and the mixture stirred until the substrate had fully dissolved. For the addition of 10 equivalents of H_2O_2 (relative to the amount of catalyst), 0.3 mL of 70 mM solution of hydrogen peroxide in acetonitrile was added dropwise over the course of 25 minutes, using a syringe pump (for the addition of 100 equivalents of H_2O_2, 0.3 ml of 700 mM solution was added over the same time). Upon completion of addition, the solution was stirred for a further 15 minutes and subsequently filtered through a pad of silica to remove the catalyst. The silica was then washed with 3.0 mL of acetonitrile and the washings combined with the filtered reaction mixture. The final concentration of the components in the reaction mixture upon the addition of 10 equivalents was: cyclohexane = 700 mM, H_2O_2 = 7mM and catalyst = 0.7 mM. This gave a substrate: oxidant: catalyst molar ratio of 1000: 10: 1. Other ratios between H_2O_2 and catalyst were obtained by adding different amounts of H_2O_2.

The acetonitrile solutions of hydrogen peroxide were prepared from commercially available 35 % aqueous hydrogen peroxide and reagent grade acetonitrile. The resultant acetonitrile solution was used without drying. The silica pads used for catalyst removal were prepared by inserting a glass wool plug into a Pasteur pipette, onto which an approximately 25 mm deep layer of silica was added.

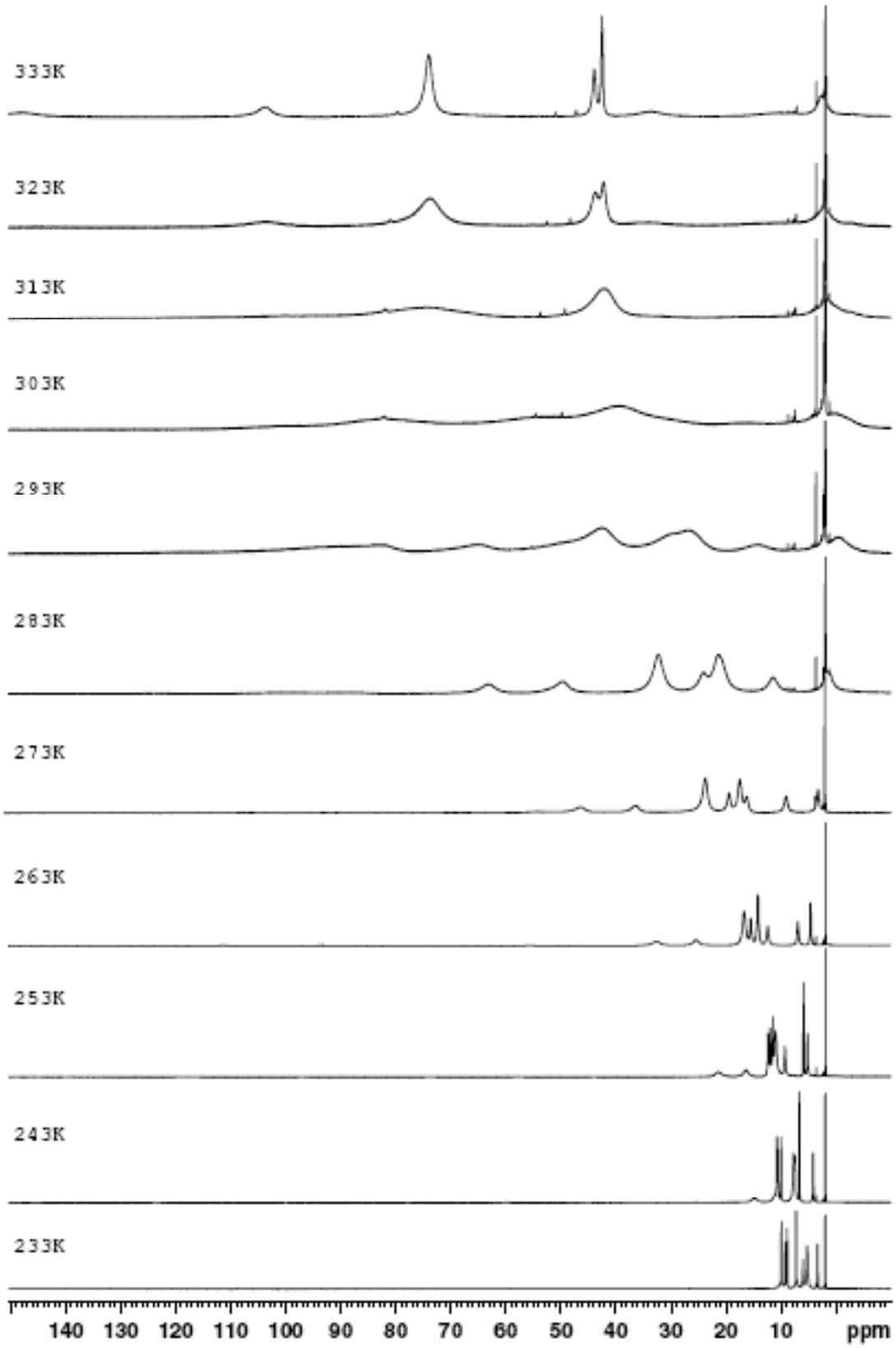


Figure S1. VT ^{1}H NMR spectra of complex [Fe(**1**)$(CD_3CN)_2$]$(OTf)_2$, recorded in CD_3CN.

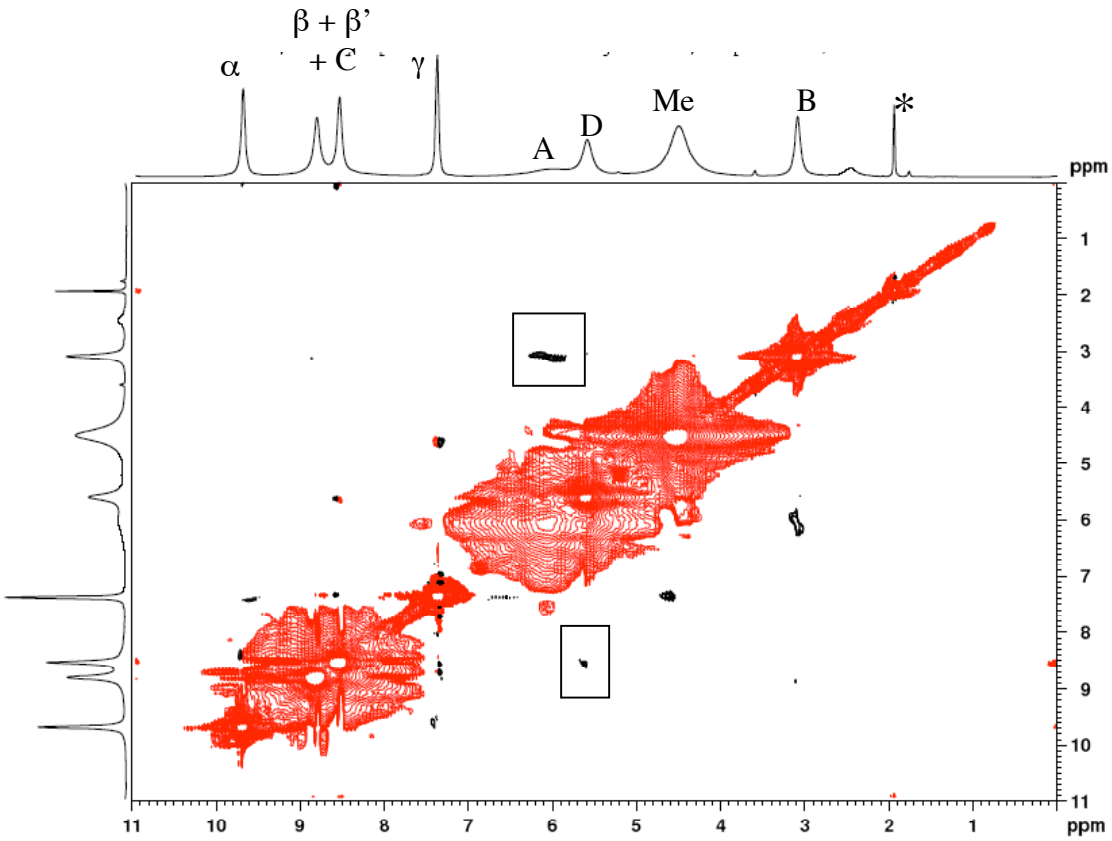


Figure S2. NOESY NMR Spectrum of [Fe(**1**)$(OTf)_2$] in CD_3CN at 226K showing cross peaks between protons A and B, and between C and D (proton C is broad like proton A and underneath protons β and β' at this temperature).

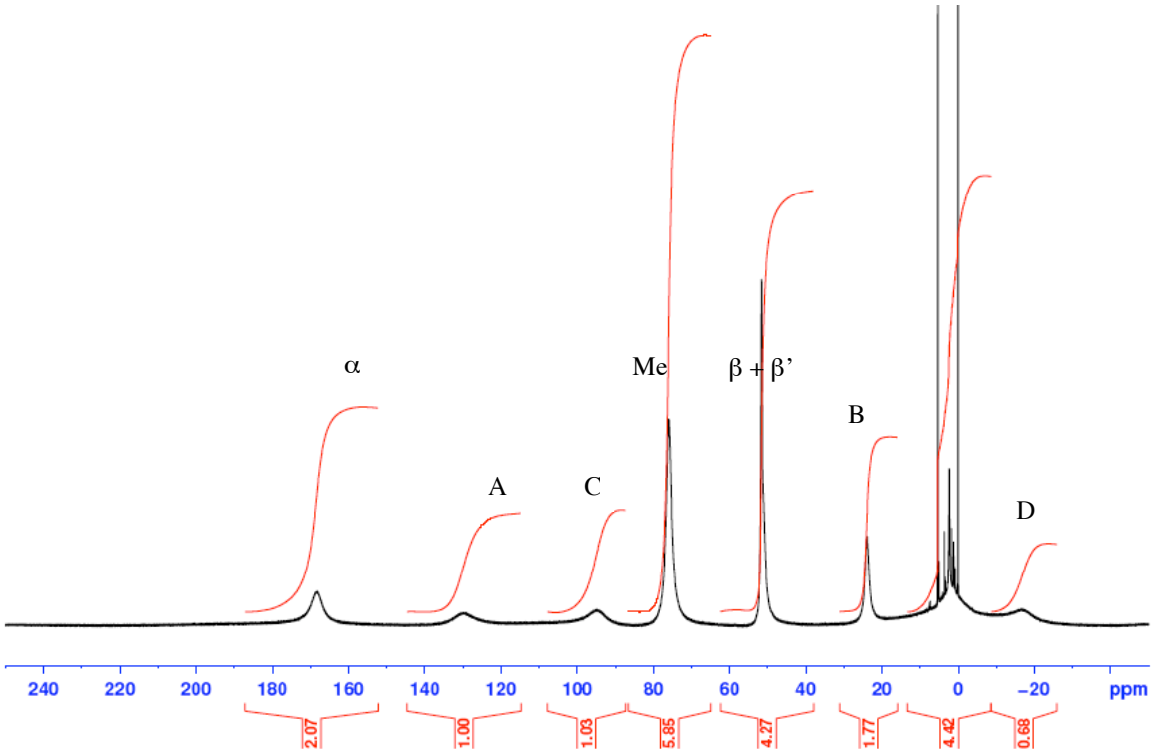


Figure S3. ^{1}H NMR spectrum of complex [Fe(**2**)(OTf)$_2$] in CD_2Cl_2 at 298 K.

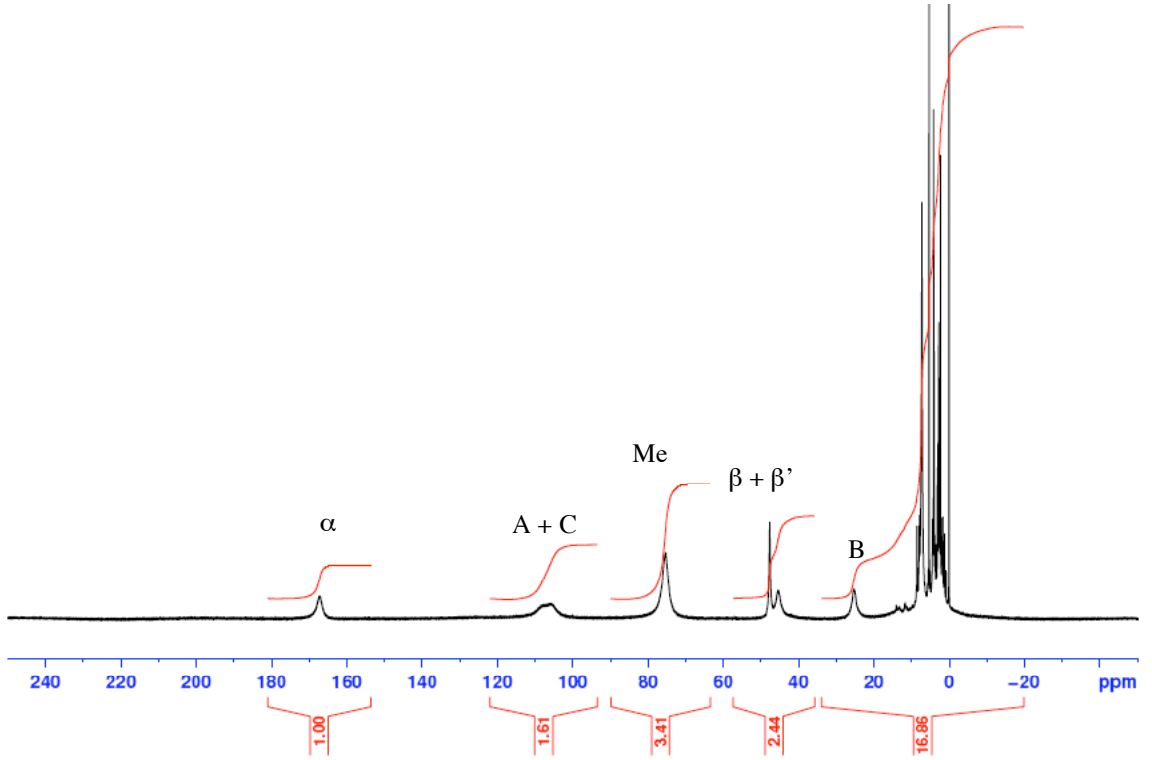


Figure S4. ^{1}H NMR spectrum of complex [Fe(**3**)(OTf)$_2$] in CD_2Cl_2 at 298 K.

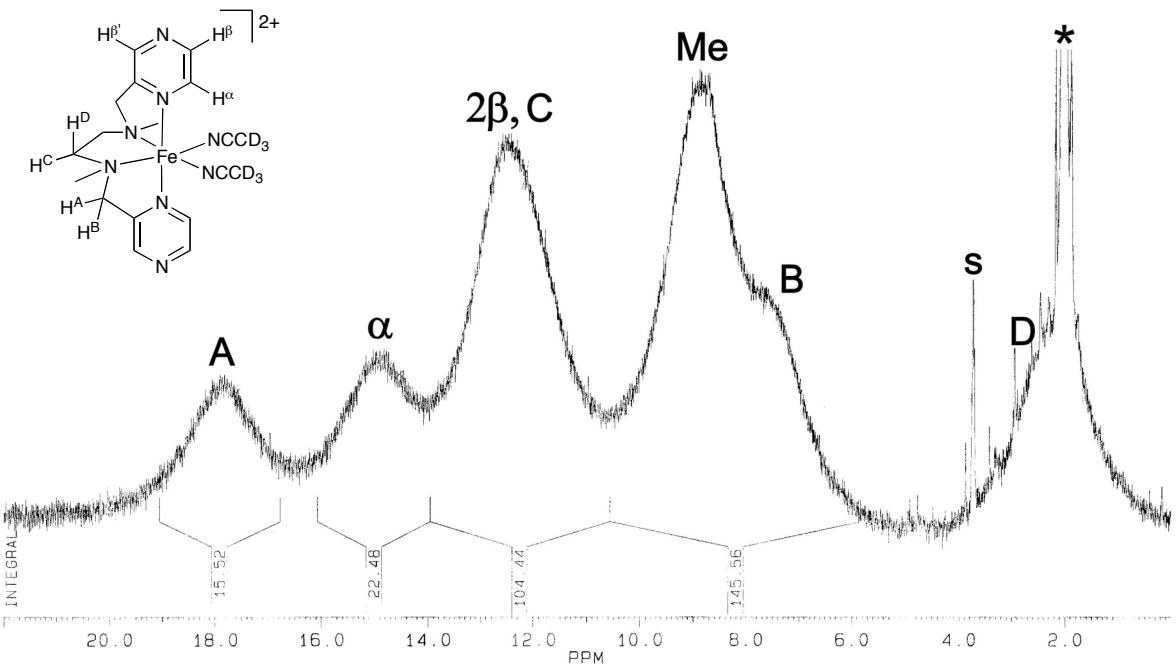


Figure S5. ^{1}H-NMR spectrum of [Fe(**4**)$(CD_3CN)_2$](OTf)$_2$, recorded in CD_3CN (∗) solution at 298 K (s: solvent residues).

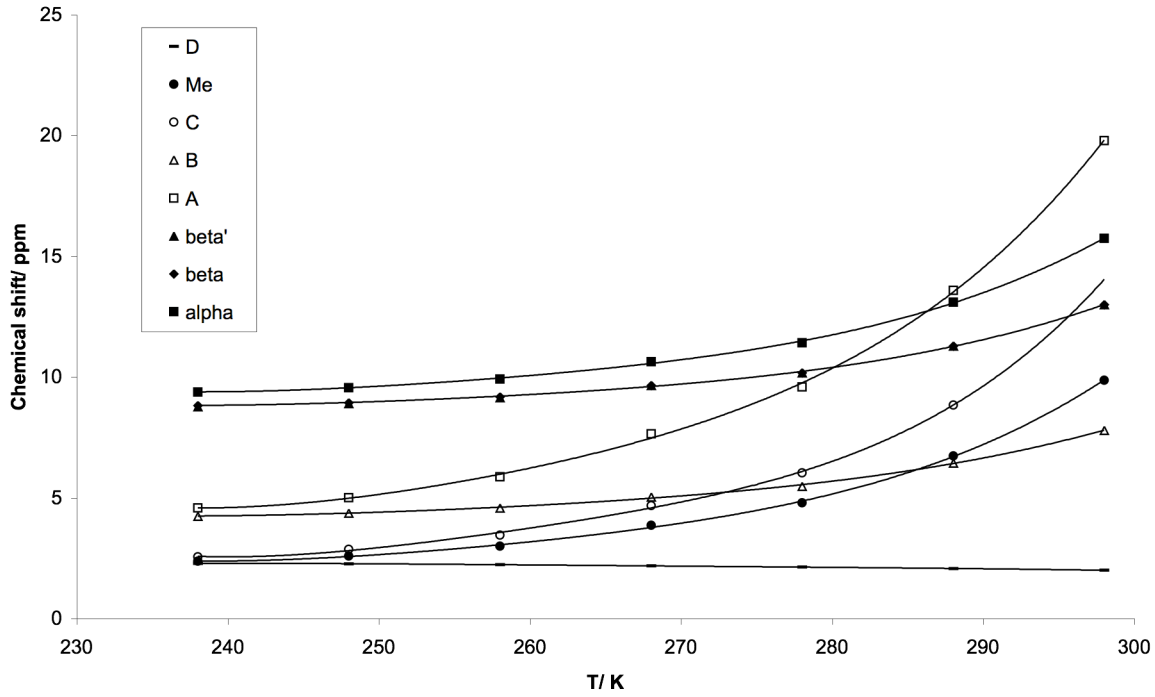


Figure S6. The variation of the ^{1}H NMR chemical shift *versus* temperature in a CD_3CN solution of [Fe(**4**)$(CD_3CN)_2$](OTf)$_2$.

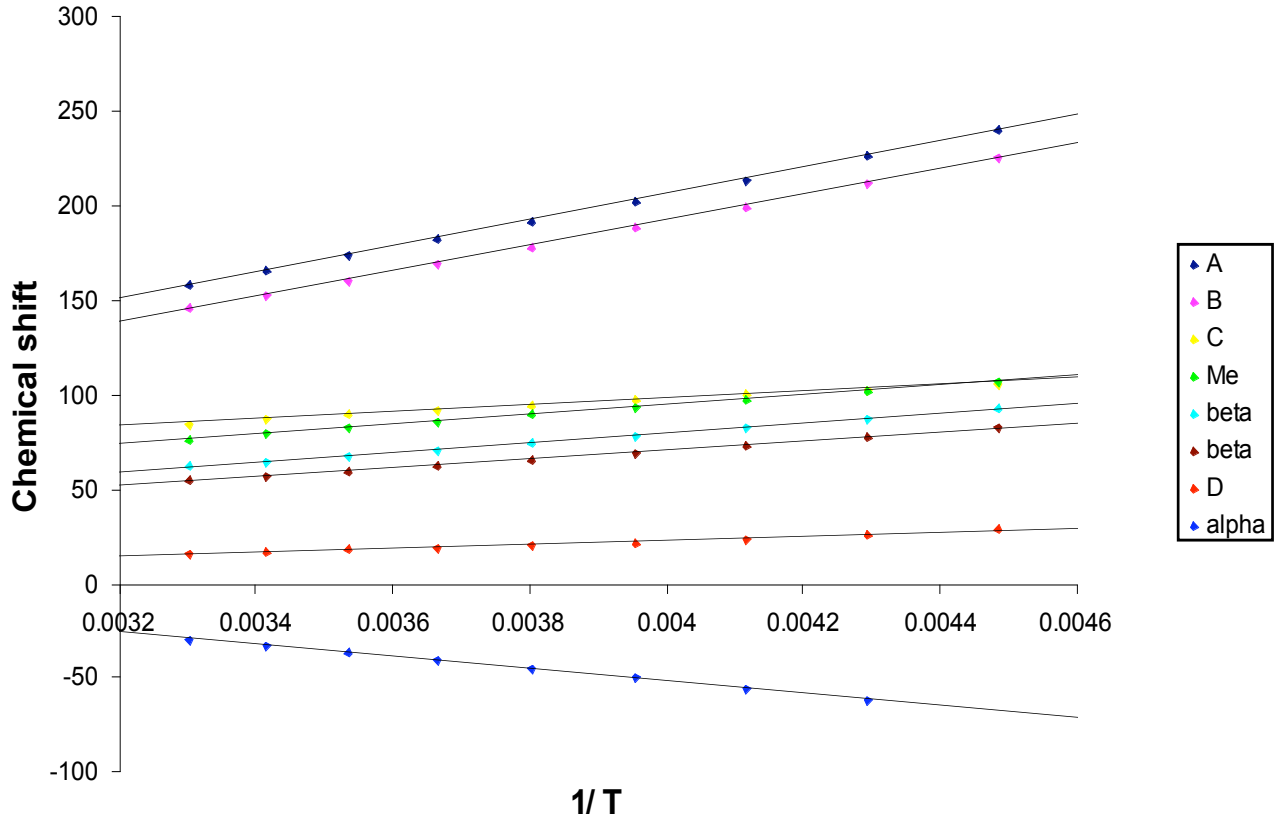


Figure S7. The variation of the ^{1}H NMR chemical shift *versus* the reciprocal of temperature in a CD_2Cl_2 solution of [Fe(**4**)$(OTf)_2$].

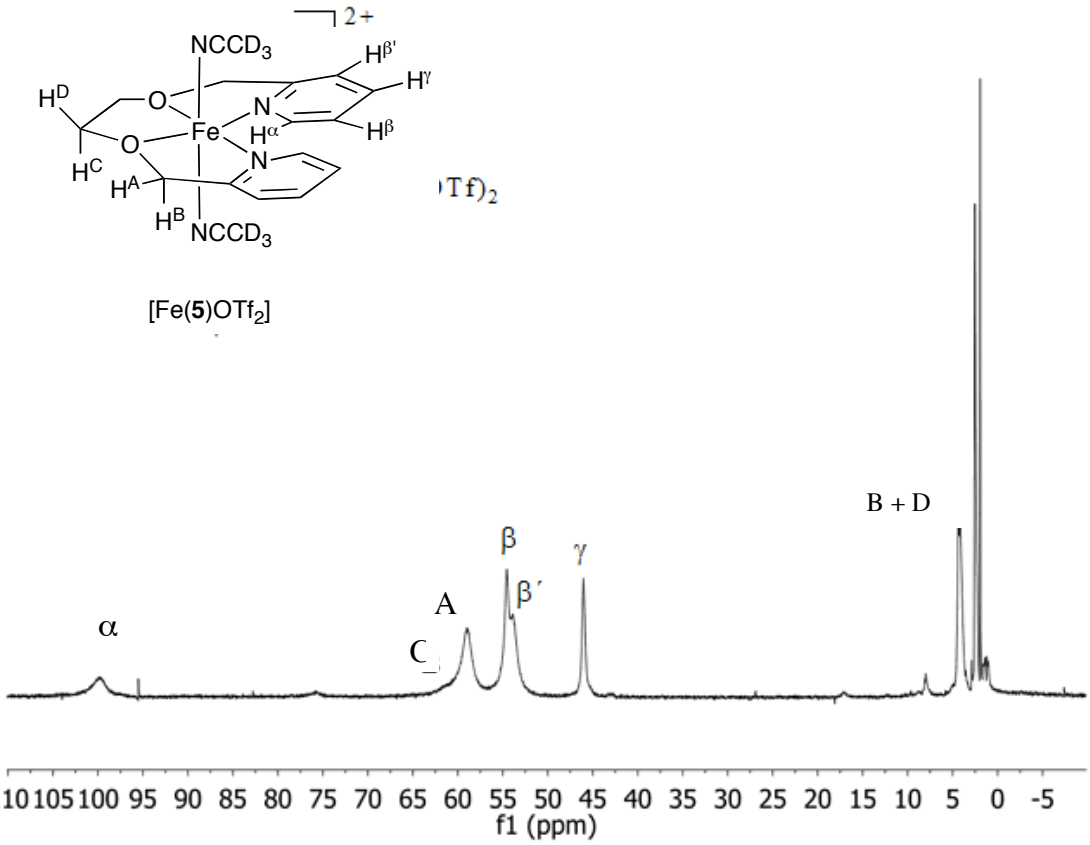


Figure S8. ^{1}H NMR spectrum of complex [Fe(**5**)(OTf)$_2$] in CD_3CN at 298 K.

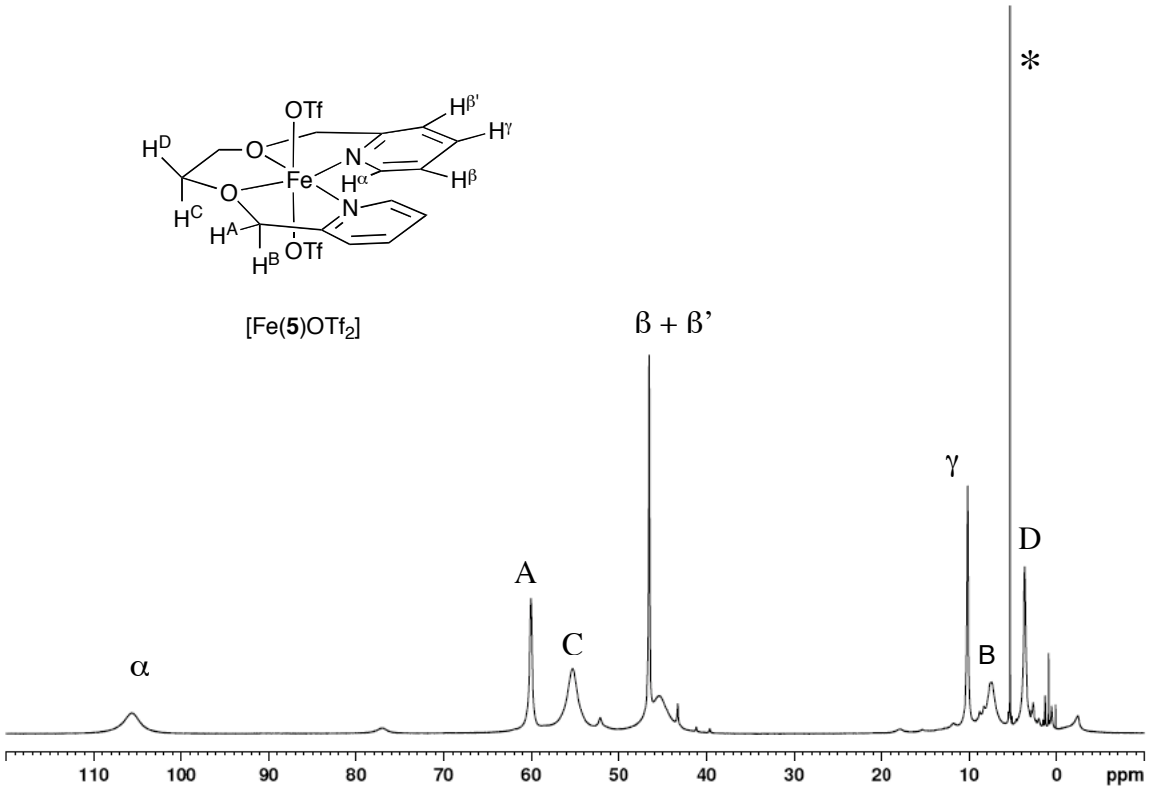


Figure S9. ^{1}H NMR spectrum of complex [Fe(**5**)$(OTf)_2$] in CD_2Cl_2 at 298 K.

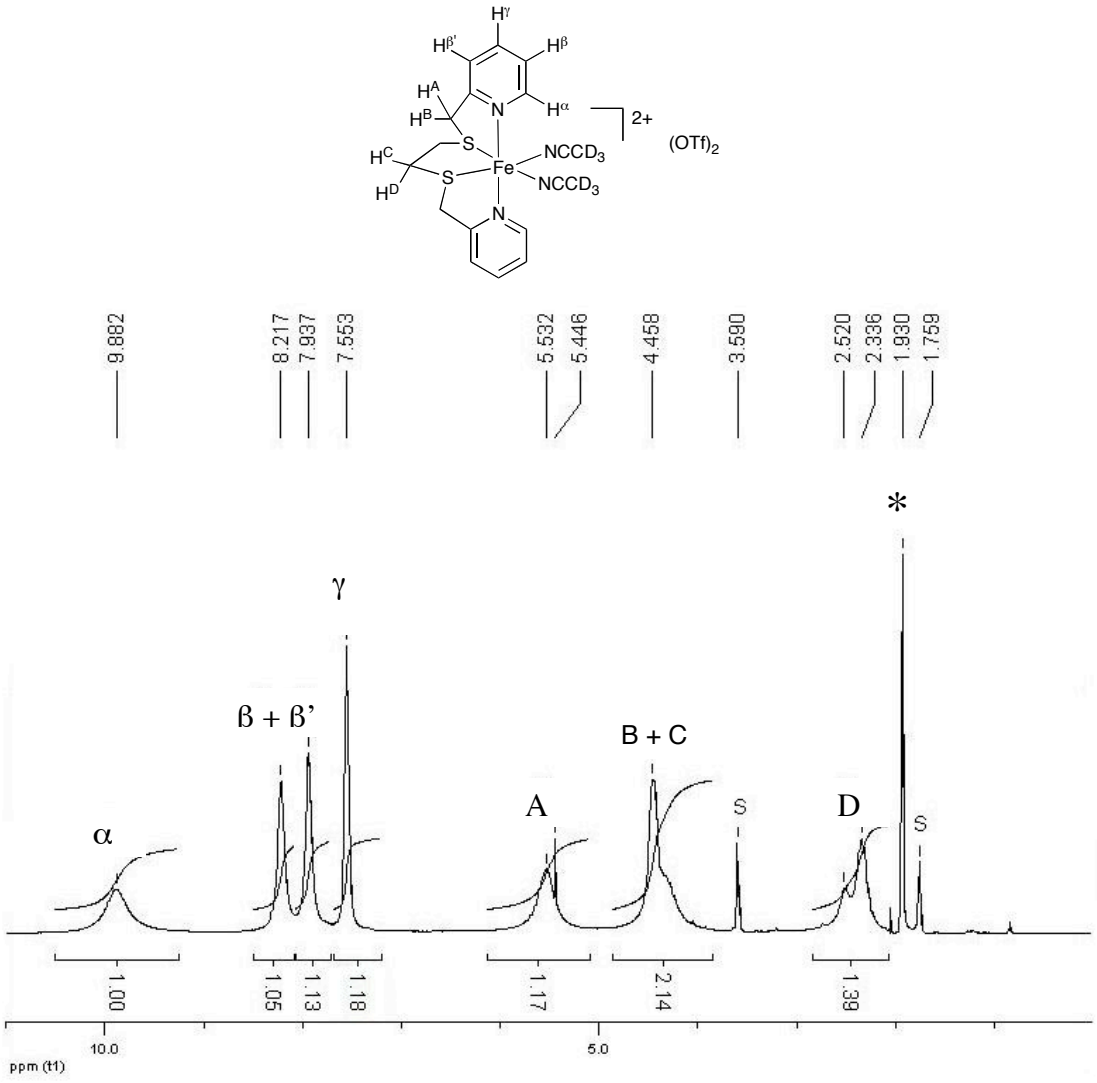


Figure S10. The ^{1}H NMR spectrum and corresponding peak assignment for [Fe(**6**)$(OTf)_2$] recorded in CD_3CN solution at 233 K. (S = solvent residues, * = CH_3CN)

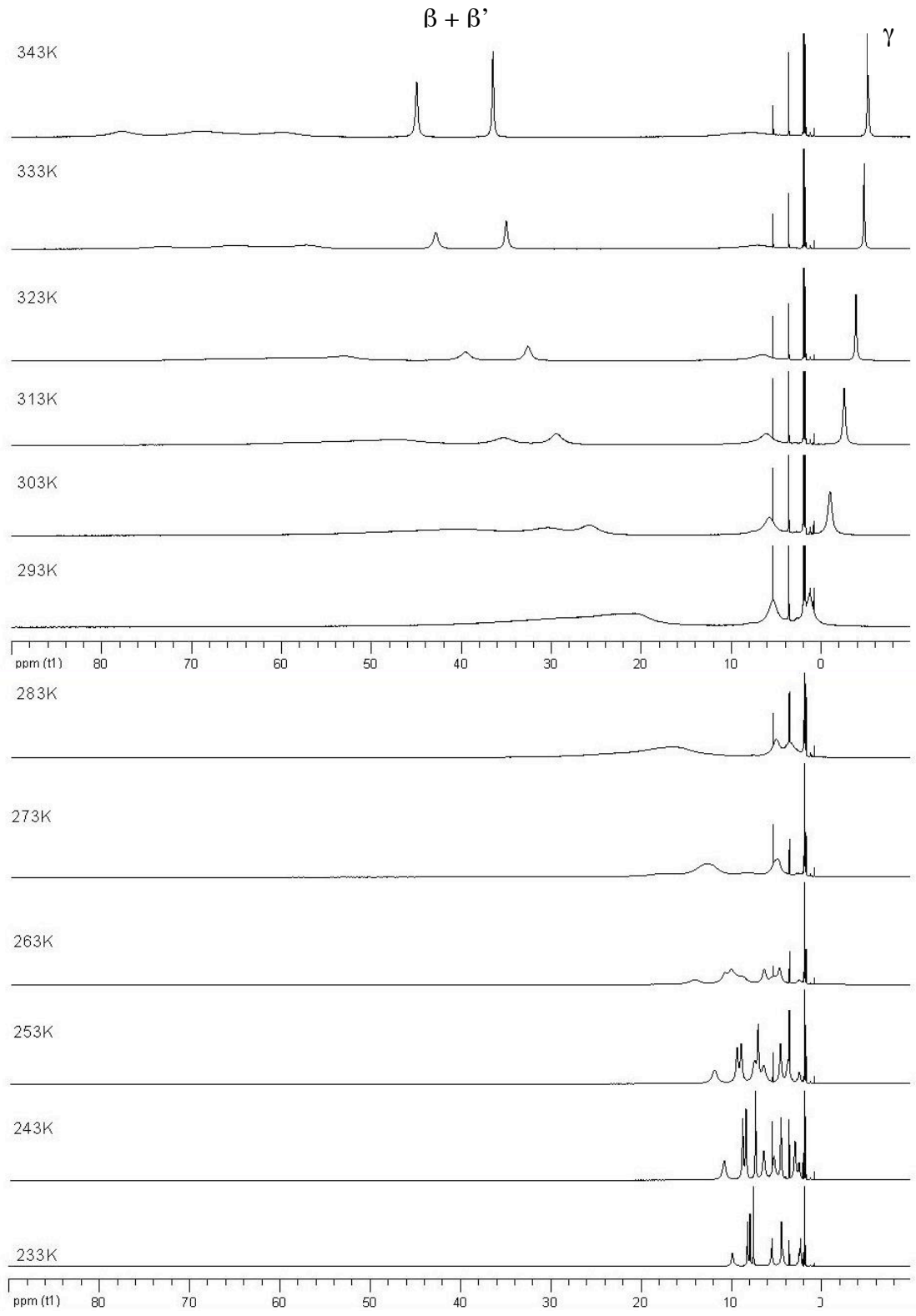


Figure S11. VT-^{1}H NMR spectra of $[Fe(\mathbf{6})(CD_3CN)_2]^{2+}$ in CD_3CN.

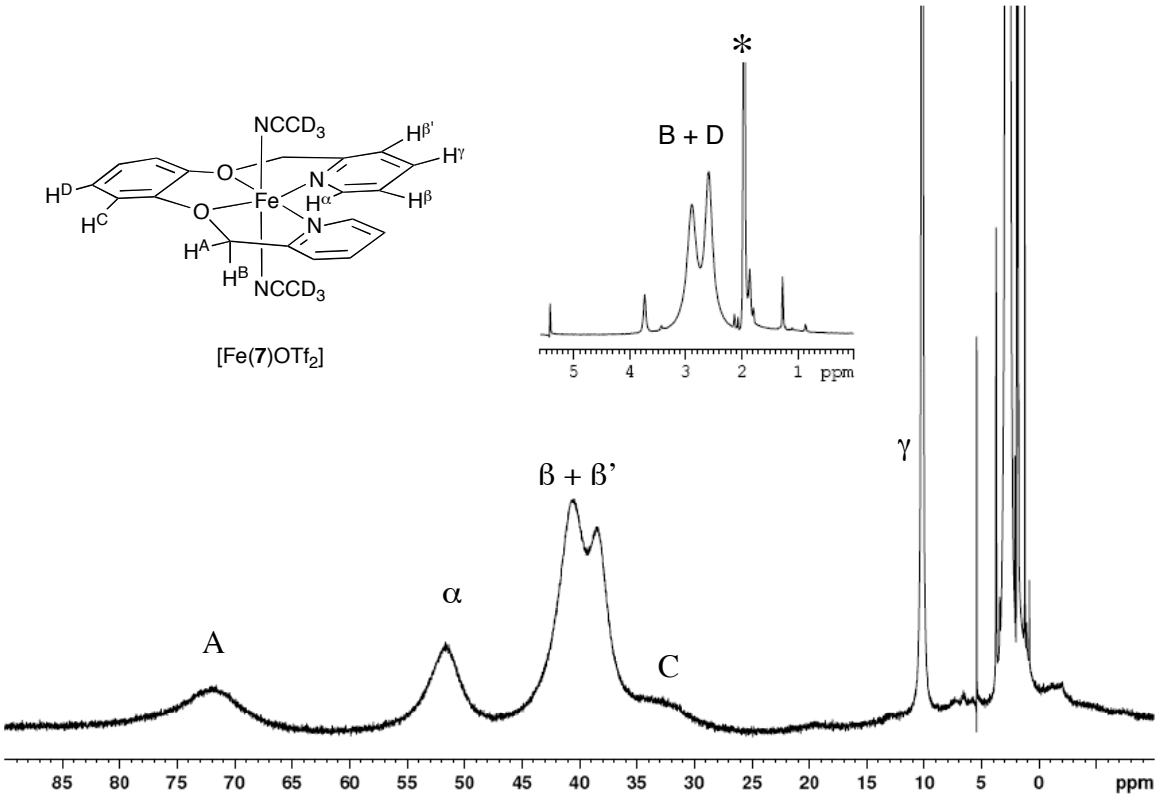


Figure S12. ^{1}H NMR spectrum of complex [Fe(**7**)(OTf)$_2$] in CD_3CN at 298 K (* = solvent).

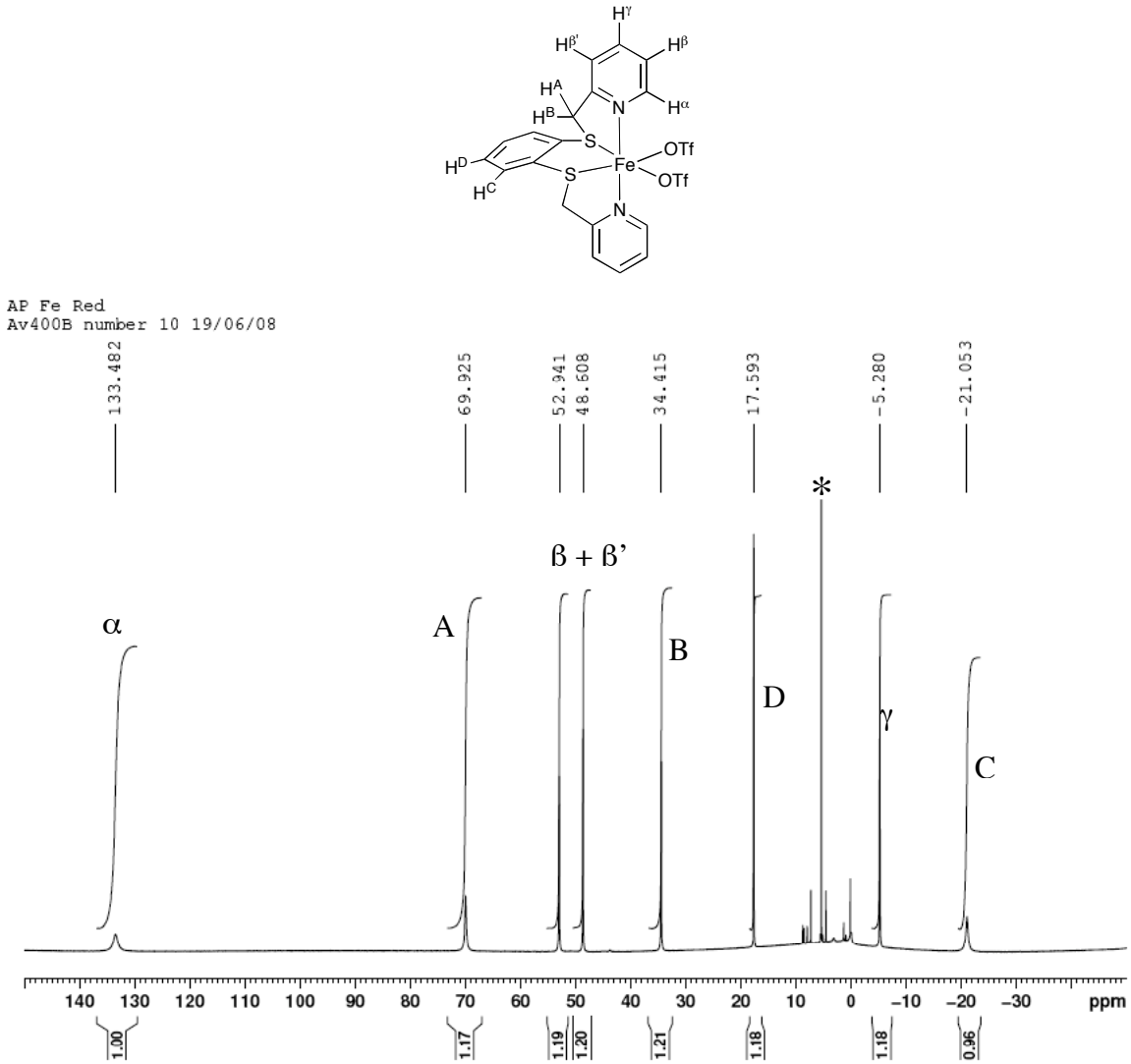


Figure S13. ^{1}H NMR spectrum of complex [Fe(**8**)$(OTf)_2$] in CD_2Cl_2 at 298 K. (* = solvent)

^{19}F NMR Spectroscopy

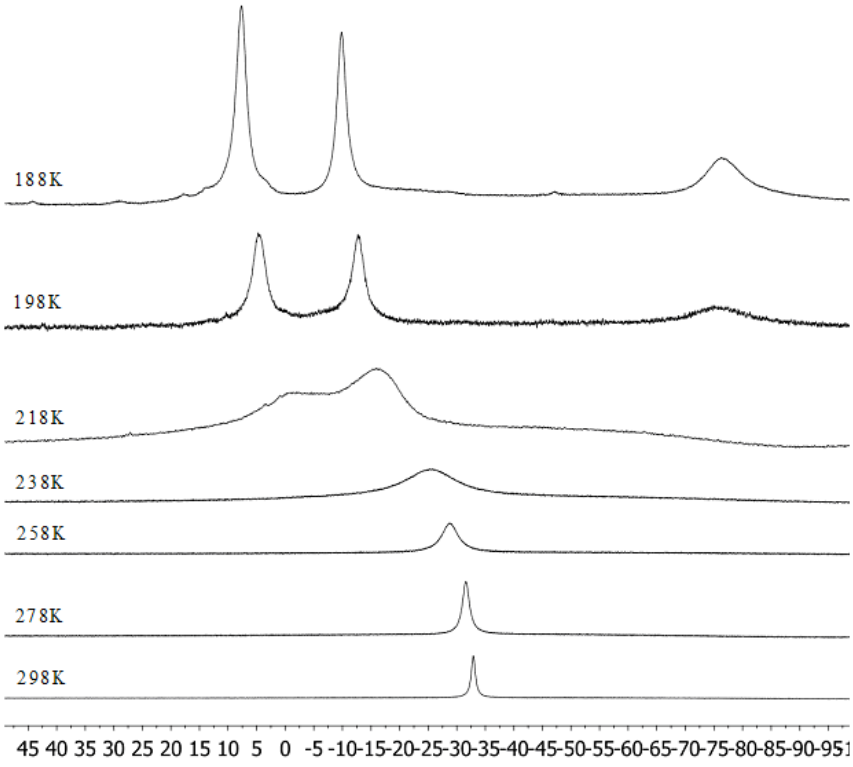


Figure S14. VT-^{19}F NMR spectra of complex [Fe(**5**)$(OTf)_2$] in CD_2Cl_2.

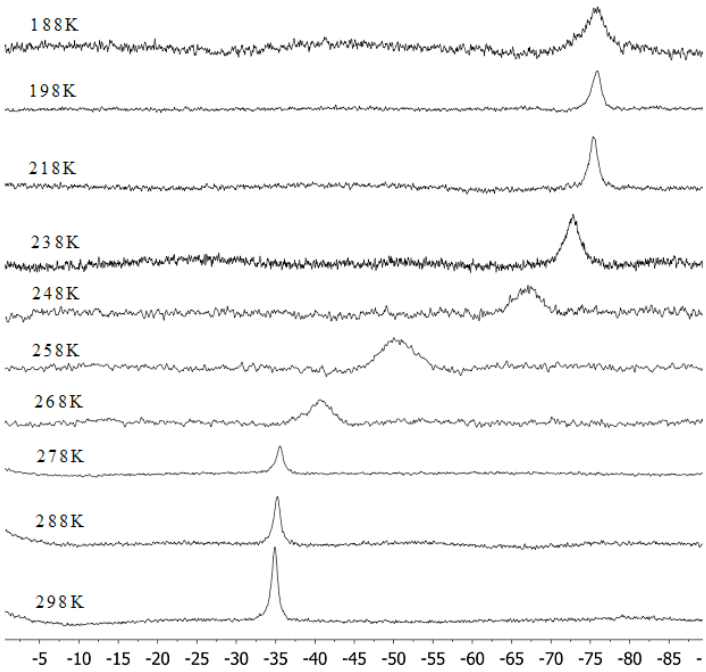


Figure S15. VT-^{19}F NMR spectra of complex [Fe(**7**)$(OTf)_2$] in CD_2Cl_2.

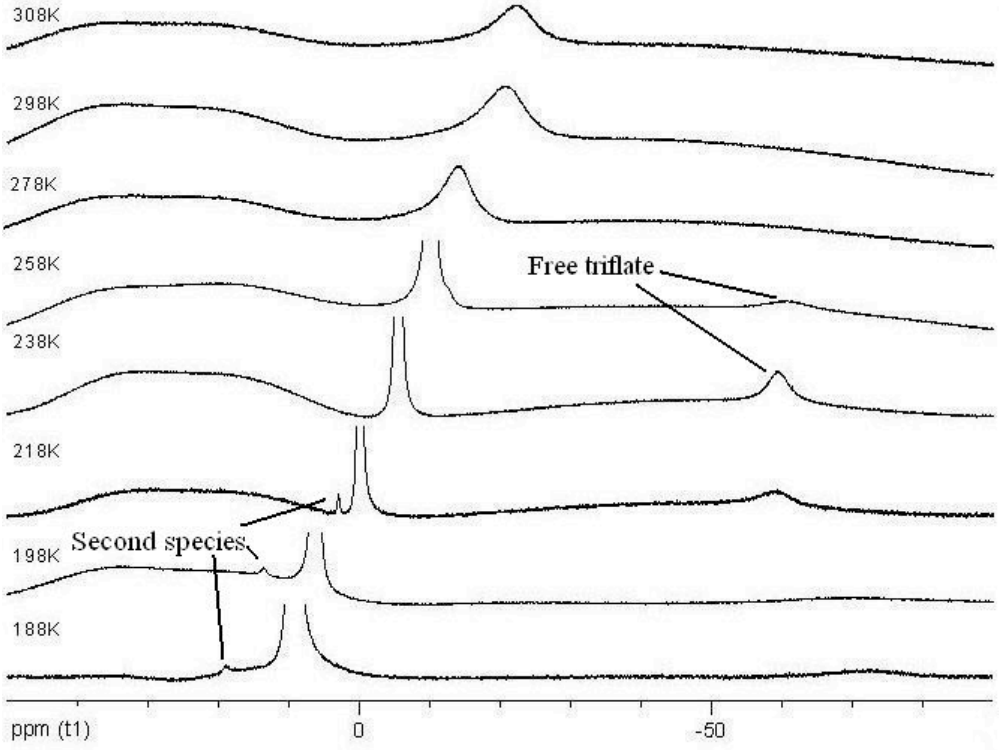


Figure S16. VT-^{19}F NMR spectra of complex [Fe(**8**)$(OTf)_2$] in CD_2Cl_2.

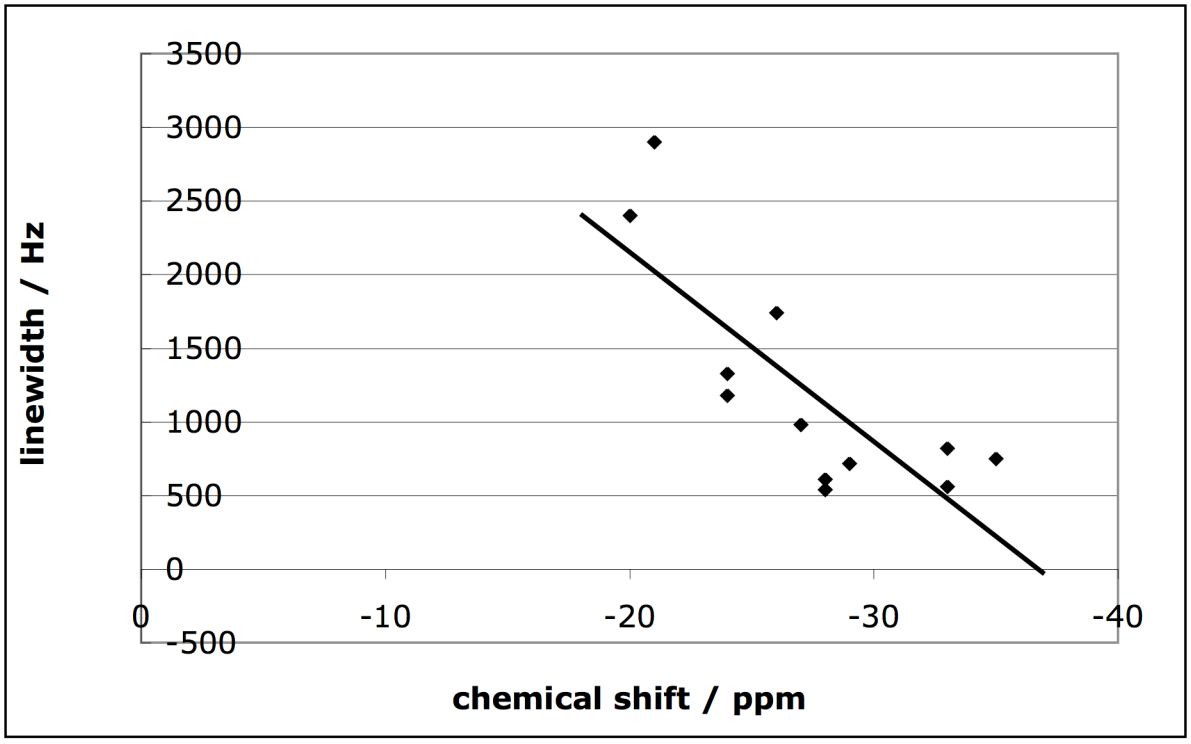


Figure S17. Correlation between the ^{19}F NMR chemical shift data and the linewidths for all complexes in CD_2Cl_2 at 298K (for data see Table 3)

Supporting Information — X-Ray Crystallography ([Fe(**6**)OTf_2]) and ([Fe(**7**)OTf_2])

During the solution and refinement of the structure of [Fe(**6**)OTf_2], there was distinct uncertainty as to the correct space group, the two choices being C2 and C2/c. When handled in the space group C2 there were found to be two crystallographically independent C_2-symmetric complexes related by an approximate centre of symmetry (Fig. S21). (The co-ordinates of the centroid of all of the unique non-hydrogen atoms of the two independent complexes are 1.00201, 0.66101, 0.74991; not surprisingly, therefore, the ADDSYM routine of PLATON suggests the presence of the c glide.) Additionally, the thermal parameters of the two independent molecules showed clear correlation effects, with the thermal ellipsoids for every atom in molecule A being larger than their counterparts in molecule B. (Though some attempts were made to address this issue in the final refinements, the effect can still be seen by comparing Figs. S18 and S20.) The chirality tests [$R_1^+ = 0.0627$, $R_1^- = 0.0628$; $x^+ = 0.49(4)$, $x^- = 0.51(4)$] suggest a racemic twin (the value of R_1 obtained when refining the Flack parameter was lower, at 0.0613).

All these above factors suggest that the correct space group is C2/c. However, reciprocal space analysis of the systematic absences was strongly against the presence of a c glide (see Table S1), and the final residuals when refined in the space group C2/c were $R_1 = 0.098$, $wR_2 = 0.241$ (c.f. $R_1 = 0.0497$, $wR_2 = 0.1283$ when refined in C_2 without any constraints on the thermal ellipsoids, vide infra), a much greater rise than one would expect from just the halving of the number of parameters.

Table S1. Reciprocal space analysis of the systematic absences for the structure of [Fe(**6**)OTf_2].

	-c-
N	310
N I>3□	263
<I>	3.8
<I/□>	44.0

In some ways the choice is a moot one, as the overall structure will be nearly identical whichever space group is chosen. In such cases the default route is to assume the presence of a centre of symmetry unless convinced otherwise. Here, the systematic absence analysis and the significantly lower residuals have been taken to be the dominant factors, and so the space group C_2 was used. In order to reduce the correlation effects between the thermal parameters of the two independent C_2 symmetric complexes, SIMU restraints were applied to each pair of pseudo-equivalent atoms [i.e. Fe with Fe', and S(8) with S(8')].

Regarding the solid state structure of complex [Fe(**7**)OTf_2], each of the pyridyl rings is approached by a fluorine atom of one of the triflate moieties. The "lower" face of the N(1) ring is approached by F(33) with an F···centroid separation of ca. 3.71 Å, whilst the "upper" face of the N(22) ring is approached by F(43) [F···centroid ca. 3.32 Å]. The other faces of both pyridyl rings are involved in intermolecular π-π stacking interactions with opposite faces of the catechol ring of adjacent complexes. For the N(1) pyridyl ring, the centroid···centroid and mean interplanar separations are ca. 4.37 and 3.57 Å respectively (the two rings being inclined by ca. 5°), whilst for the N(22) pyridyl ring, the centroid···centroid and mean interplanar separations are ca. 3.84 and 3.52 Å respectively (the two rings being inclined by ca. 12°). The two centroid···centroid vectors subtend an angle of ca. 165° at the

catechol ring centroid, and these π-π interactions serve to form a chain of molecules along the crystallographic 101 direction.

Fig. S18 The molecular structure of one (A) of the two crystallographically independent C_2 symmetric complexes present in the crystals of [Fe(**6**)OTf_2] (50% probability ellipsoids).

Fig. S19 The molecular structure of one (B) of the two crystallographically independent C_2 symmetric complexes present in the crystals of [Fe(**6**)OTf_2].

Fig. S20 The molecular structure of one (B) of the two crystallographically independent C_2 symmetric complexes present in the crystals of [Fe(**6**)OTf_2] (50% probability ellipsoids).

Fig. S21 The asymmetric unit in the structure of [Fe(**6**)OTf_2] showing the approximate centrosymmetric arrangement of the two independent C_2 symmetric complexes.

Fig. S22 The molecular structure of [Fe(**7**)OTf_2] (50% probability ellipsoids).

Fig. S23 Histogram showing the results of a search of the Cambridge Structural Database (version 5.29, Jn-2008 update) for Fe–S bond lengths in iron thioether complexes.

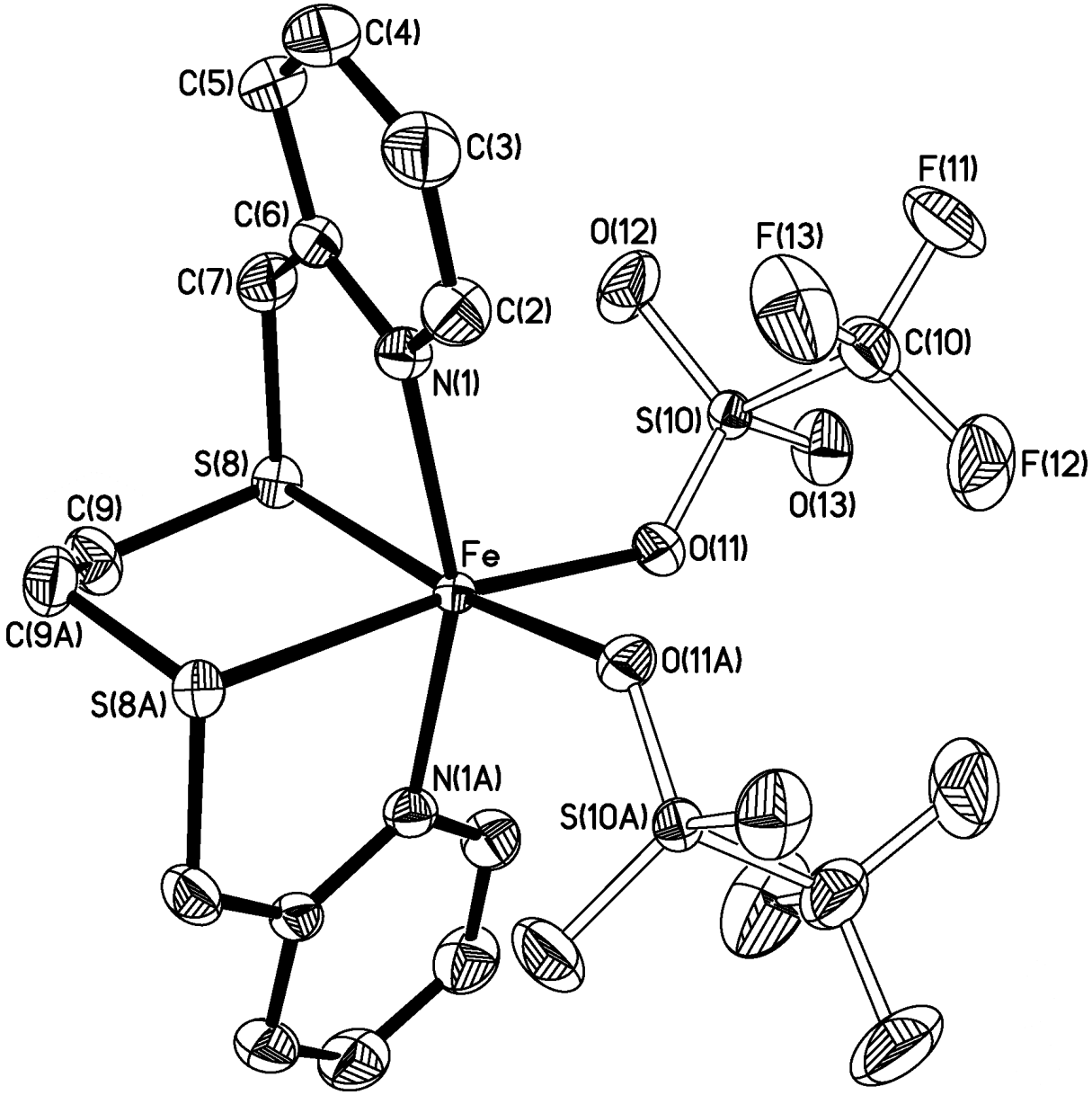

C(4)
C(5)
C(3)
C(6)
C(7)
C(2)
N(1)
S(8)
C(9)
C(9A)
S(8A)
Fe
O(11)
O(11A)
N(1A)
S(10A)
O(12)
F(13)
F(11)
C(10)
S(10)
O(13)
F(12)

Fig. S18

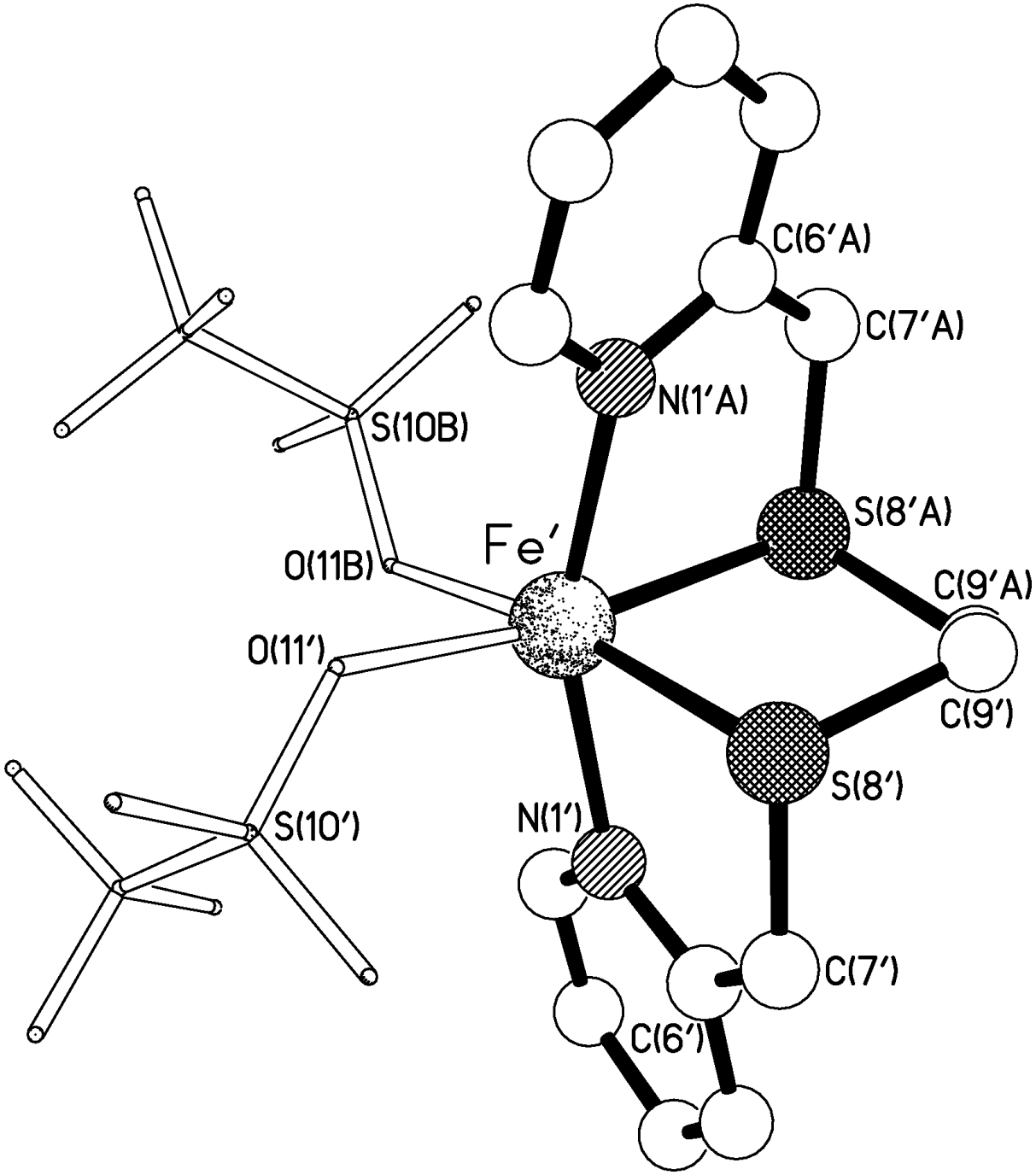


Fig. S19

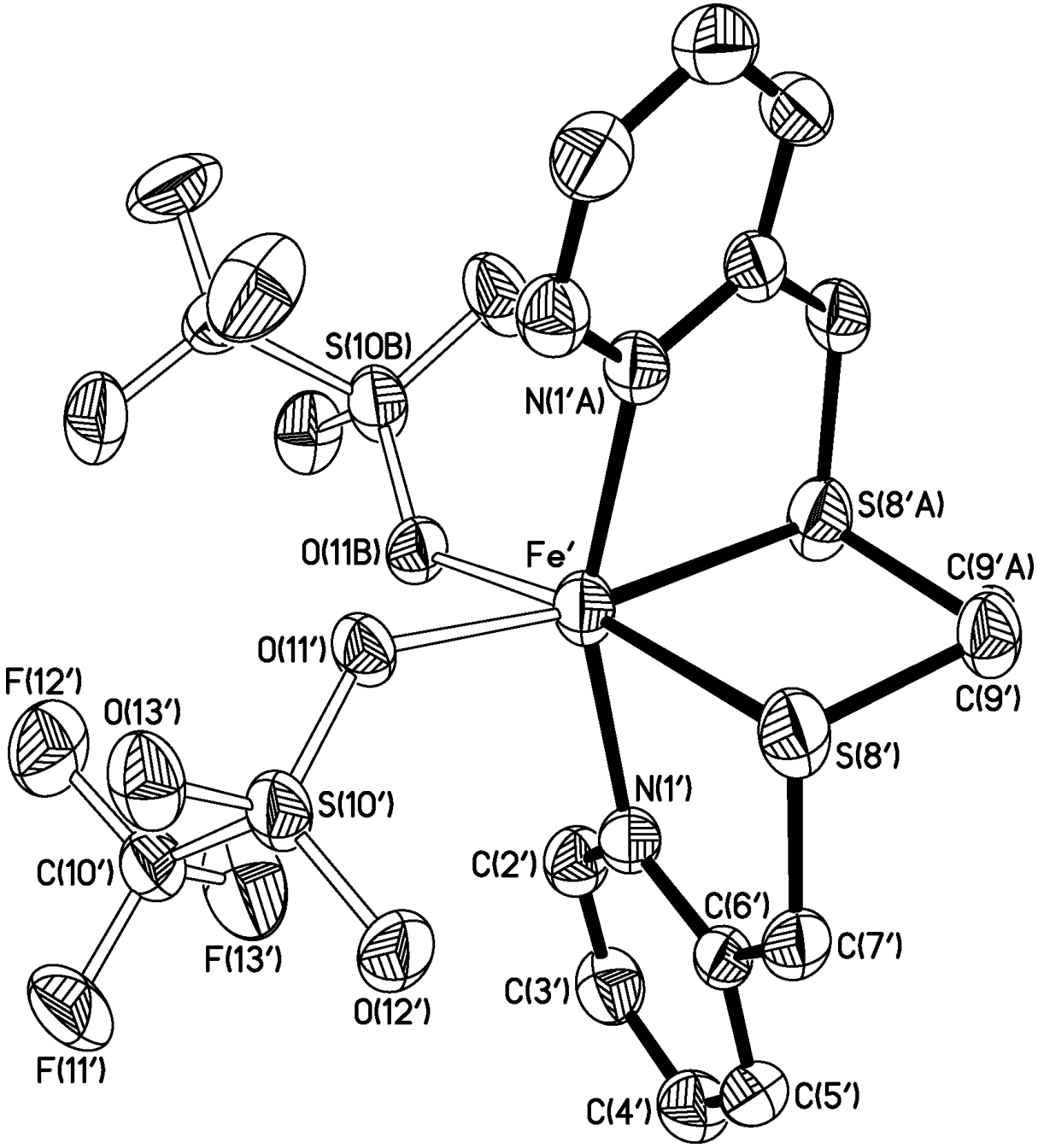

S(10B)
N(1'A)
S(8'A)
O(11B)
Fe'
C(9'A)
O(11')
C(9')
F(12')
O(13')
S(8')
S(10')
N(1')
C(10')
C(2')
C(6')
C(7')
F(13')
C(3')
O(12')
F(11')
C(4')
C(5')

Fig. S20

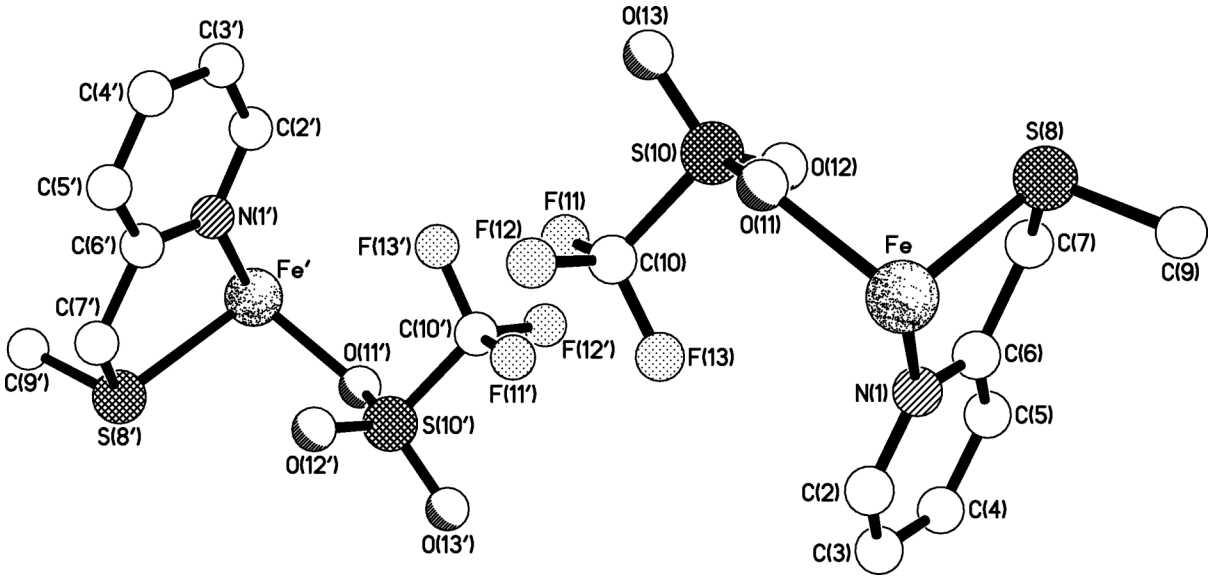

C(3′)
C(4′)
C(2′)
C(5′)
N(1′)
C(6′)
Fe′
C(7′)
C(9′)
S(8′)
O(11′)
C(10′)
F(13′)
F(12′)
F(11′)
S(10′)
O(12′)
O(13′)
O(13)
S(10)
O(12)
F(11)
F(12)
O(11)
C(10)
F(13)
Fe
S(8)
C(7)
C(9)
C(6)
N(1)
C(5)
C(2)
C(4)
C(3)

Fig. S21

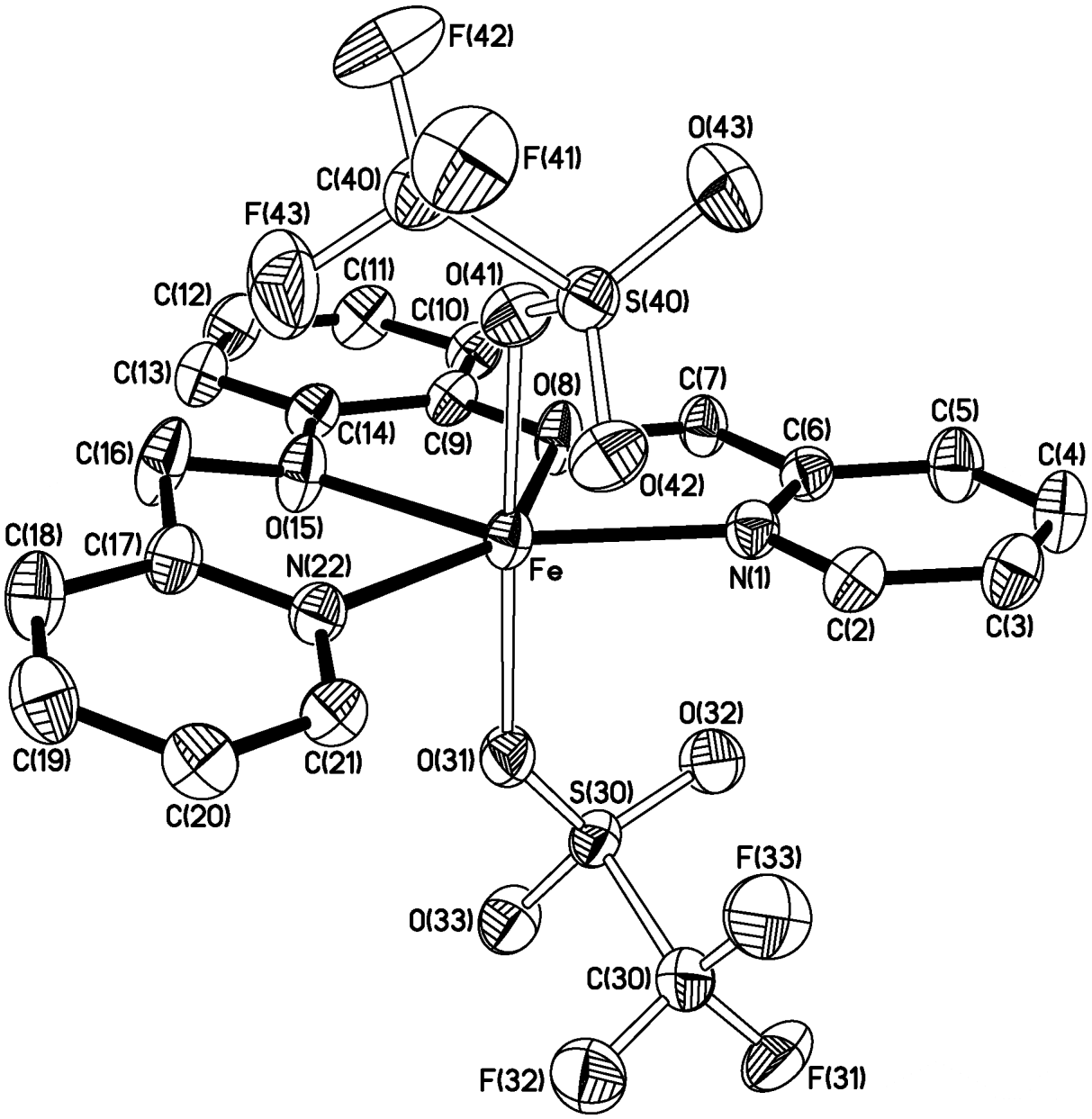

F(42)
F(41)
O(43)
C(40)
F(43)
C(11)
O(41)
C(12)
C(10)
S(40)
C(13)
O(8)
C(7)
C(5)
C(14)
C(9)
C(6)
C(4)
C(16)
O(42)
O(15)
C(18)
C(17)
N(22)
Fe
N(1)
C(2)
C(3)
O(32)
C(19)
O(31)
C(21)
S(30)
C(20)
F(33)
O(33)
C(30)
F(32)
F(31)

Fig. S22

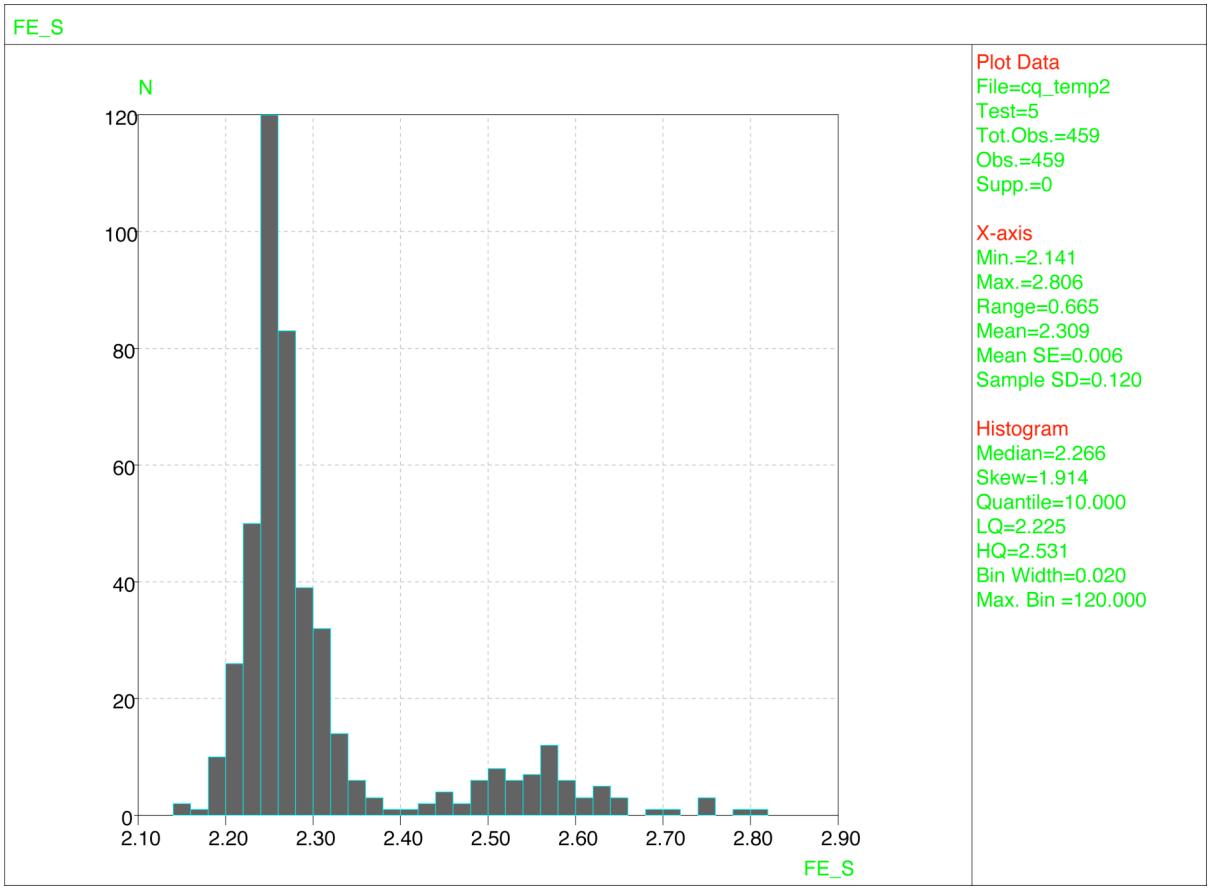

FE_S
N
120
100
80
60
40
20
0
2.10
2.20
2.30
2.40
2.50
2.60
2.70
2.80
2.90
FE_S
Plot Data
File=cq_temp2
Test=5
Tot.Obs.=459
Obs.=459
Supp.=0
X-axis
Min.=2.141
Max.=2.806
Range=0.665
Mean=2.309
Mean SE=0.006
Sample SD=0.120
Histogram
Median=2.266
Skew=1.914
Quantile=10.000
LQ=2.225
HQ=2.531
Bin Width=0.020
Max. Bin =120.000

Fig. S23